

Comparative Analysis of the Physical and Chemical Properties of Different Biomass Ashes Produced from Various Combustion Conditions

Xiwen Yao,^a Kaili Xu,^{a,*} and Yu Liang^b

The ash yield, composition, mineral phases, and other physical and chemical properties of various biomass ashes are dependent on ashing temperature. To fully understand the impacts of biomass species and ashing temperature on the characterization of biomass ashes, three kinds of biomass fuels were treated at different ashing temperatures to produce biomass ashes. Their properties were analyzed by a series of qualitative and quantitative methods, including X-ray fluorescence (XRF), X-ray diffraction (XRD), scanning electron microscopy (SEM), energy dispersive X-ray (EDX), thermal gravimetric, and differential thermal analyzer (TG-DTA). The experimental results indicated that as the ashing temperature was raised, the ash slagging tendency could be enhanced. The fused layer on the surface of ash particles was coated with potassium chloride, which was the key reason for the development of severe agglomeration and slagging. Due to the high carbon content and large number of pores in the lower temperature ashes, a low-cost adsorbent could be developed effectively from these carbon materials. The thermal decomposition of all ashes showed a stepwise mechanism. The total weight loss of the same biomass ash decreased with increased ashing temperature, which corresponded well with the phase transitions and thermal reaction sequences.

Keywords: Biomass waste; Fly ash; Combustion; Characterization; Slagging; Applications

Contact information: a: School of Resources and Civil Engineering and b: College of Information Science and Engineering, Northeastern University, Shenyang 110819, PR China;

* Corresponding author: neu_kailixu@126.com

INTRODUCTION

Due to the depletion of fossil fuels and the increasing severity of environmental problems, biomass fuels have gained increasing popularity as an environmentally friendly source of energy (Rizvi *et al.* 2015). Every year, significant amounts of crop residues are produced as a byproduct of the processing of various agricultural commodities. In many cases, these agricultural byproducts are treated as waste materials with little or no economic value, and their disposal is sometimes costly and environmentally harmful (Rehrah *et al.* 2014). A variety of agriculture residues have been studied for their possible use as renewable fuels, and these agricultural residues are freely available for use as fuel in rural areas, although they are also responsible for air pollution (Motghare *et al.* 2016). Thermo-chemical processes such as gasification, liquefaction, pyrolysis, and direct combustion are commonly employed for converting biomass wastes into higher heating value fuels (McKendry 2002; Haykiri-Acma *et al.* 2013).

After thermal-chemical processing, however, there still exist relatively large quantities of inorganic elements (including potassium, sodium, calcium, phosphorus, *etc.*) in the ash (Wang *et al.* 2008; Xiao *et al.* 2011). Biomass ash is easy to melt and volatilize because of the presence of these inorganic elements (Arvelakis *et al.* 2004). Thus, the types of biomass ash with relatively high volatility and complex composition often easily and problematically result in slagging, fouling, and corrosion; these problems are closely related to the high content of alkali metal and alkali earth metals (Knudsen *et al.* 2004; Xiao *et al.* 2011). Moreover, the primary properties of biomass ashes can significantly influence their potential utilization in various fields as well as affect the products of biomass gasification, combustion, and pyrolysis. Therefore, from both an economic and environmental point of view, it is meaningful to investigate the physico-chemical and slagging characteristics of biomass ash.

Considering the biomass availability and area-specific agriculture residues together with the related transportation costs, it is important to explore various local biomasses for their suitability as a biomass fuel. There have been numerous studies characterizing various biomass ashes, such as seaweed biomass ash (Wang *et al.* 2008), woody biomass ash (Skrifvars *et al.* 2004), bagasse fly ash (Batra *et al.* 2008), cashew nut ash (Ogundiran *et al.* 2011), wheat hull ash (Terzioğlu *et al.* 2013), peanut hull ash (Liao *et al.* 2011), sunflower husk ash (Quaranta *et al.* 2011), corn straw ash, and bamboo ash (Fang and Jia 2012).

These investigations revealed that the physicochemical properties of various biomass ashes are quite different. In addition, there have been research efforts on various potential utilizations of biomass ashes, including as a soil amendment (Pan and Eberhardt 2011), a raw material for ceramic production (Abraham *et al.* 2013), a potential source of SiO₂ (Terzioğlu *et al.* 2013), as well as a bio-based materials for biopolymers (Burgos *et al.* 2016), and so on.

However, in comparison with coal fly ash, on which notable research has already taken place and high utilization figures have already been reported (Kutchko and Kim 2006; Blissett and Rowson 2012), the influences of ashing temperature and biomass species on the preliminary characterization and applications of various biomass ashes have been neither widely researched nor reported and are still incompletely understood or uncertain in many details. For this reason, further relevant studies are needed.

The overall objectives of this study were to determine the influences of ashing temperatures and biomass species on the ash yield, composition, mineral phases, and such physical and chemical properties of biomass ashes that serve as predictors of suitability in their potential uses.

This study provides referable information for the efficient use of the waste ashes in various industries. In this paper, the physicochemical properties of biomass ashes from three types of biomass widely available around the world (rice straw, peanut shell, and corn cob) were comprehensively characterized in terms of their potentials to be transformed into eco-friendly and some high value-added products. To accurately determine the properties of biomass ashes and fully understand the impacts of ashing temperatures on their characterization, a series of qualitative and quantitative analysis methods were employed, including X-ray fluorescence (XRF), X-ray diffraction (XRD), scanning electron microscopy (SEM), energy dispersive X-ray (EDX), and thermal gravimetric and differential thermal analyzer (TG-DTA).

EXPERIMENTAL

Biomass Samples Preparation

The rice straw, peanut shell, and corncob material used in preparation of the biomass ashes were obtained from the peripheral rural area of Shenyang, in northeast China. Prior to ash preparation, all biomass samples were oven-dried at 105 ± 0.5 °C for 24 h, ground in a high-speed rotary cutting mill, and sieved with a 100-mesh sieve. The samples that passed through the sieve were collected in a closed vessel and retained for analysis. Table 1 shows the general characterization of the biomass samples.

Table 1. General Characterization of Biomass Samples (on Air-dried Basis)

Materials	Proximate Analysis (wt.%)			Ultimate Analysis (wt.%)					
	Volatile Matter	Moisture	Fixed Carbon	Ash	C	H	O	N	S
Rice straw	72.43	1.38	14.37	11.82	43.89	5.18	36.37	1.25	0.11
Peanut shell	71.36	1.16	20.67	6.81	46.15	5.62	38.25	1.89	0.12
Corn cob	79.25	0.87	17.64	2.24	47.26	5.79	43.23	0.56	0.05

Biomass Ashes Preparation

No specific standards are available in China for the preparation of biomass ash. Hence, the ashing temperatures of the prepared biomass samples (rice straw, corncob, and peanut shell) were set at 600 and 815 °C, according to the ASTM E1755-01 standard (2015) and according to the Chinese National Bureau of Standards for coal ash preparation (GB/T212 2008). In accordance with previous literature (Wang *et al.* 2008), the ashing temperature of seaweed biomass was approximately 500 °C. To increase the validity of this research, these pulverized samples were placed in a muffle furnace (SX2-15-12, Dongtai Shuangyu Instruments Co., Ltd., Jiangsu, China) and kept for 2 h at temperatures of 500, 600, and 815 °C. The storage interval of the furnace was 1 °C, and the atmosphere was air. The biomass ashes obtained at 500 °C were light black, indicating that there was still residual char in the ash because the biomass had incompletely combusted at this lower temperature (Xiao *et al.* 2011). The rice straw ash (RSA) and corncob ash (CCA) obtained at 600 °C were light grey, while the RSA and CCA obtained at 815 °C were dark grey and seriously sintered, which reveals that the rice straw and corncob were relatively easy to slag during the ashing process. The peanut shell ash (PSA) obtained at 600 °C was light khaki and loose, while those obtained at 815 °C were dark khaki and compacted. All ash samples were collected in an airtight container for further analysis.

Ash Characteristic Measurements

The chemical composition of biomass ash was obtained by using XRF (ZSX100e, Rigaku Co., Tokyo, Japan). The main crystalline compounds were identified using XRD (X'Pert PRO, PANalytical B.V., Almelo, Netherlands) with Cu K α radiation ($\lambda = 0.15406$ nm) at a scan rate of 0.02°/s. The surface morphology was observed using SEM (Ultra Plus, Carl Zeiss Co. Ltd., Oberkochen, Germany) with an accelerating voltage of 20 to 30 kV. The ash surface composition was analyzed using EDX (Genesis, Edax DX-4) at an accelerating voltage of 25 kV.

The simultaneous thermal analysis (STA) on biomass ashes was performed using a simultaneous thermogravimetric analyzer (NETZCH-STA449 F3, Selb, Germany) to obtain the weight loss and using a differential thermal analyzer (DTA) to acquire the phase transition as a function of temperature. The sensitivity of the thermogravimetric analyzer was 1 μg and 0.01 $^{\circ}\text{C}$. The biomass ash samples used for each test were 5 mg. The temperature range was from room temperature (approximately 25 $^{\circ}\text{C}$) to 1200 $^{\circ}\text{C}$ at a heating rate of 20 $^{\circ}\text{C}/\text{min}$. The heating was carried out in dry air. The flow rate of carrier gas was 30 mL/min. Each experiment was carried out at least three times.

RESULTS AND DISCUSSION

Determination of Ash Yield

Table 2 shows the ash yield of biomass at different ashing temperatures. In order to check the reproducibility of the experiments, at least three runs were carried out for each set of parameters under the same experimental condition. The data presented good reproducibility, with a standard deviation of less than 1%.

Table 2. Ash Contents of Different Biomass at Different Temperatures (wt.%)

Temperature ($^{\circ}\text{C}$)	Rice Straw	Corn cob	Peanut Shell
500	13.05	12.51	8.67
600	9.48	8.54	5.23
815	8.69	7.83	4.05

For each biomass, the ash yield declined with the increase of ashing temperature. The ash yield at 500 $^{\circ}\text{C}$ was higher than those at 600 and 815 $^{\circ}\text{C}$, indicating that at 500 $^{\circ}\text{C}$ there were still combustible substances in the incompletely combusted biomass. Therefore, 500 $^{\circ}\text{C}$ was not suitable for preparing biomass ashes, and the ashes generated at 600 and 815 $^{\circ}\text{C}$ were used in further analyses. These findings corresponded well with Xiao *et al.* (2011), who measured the ash contents of rice straw, pine sawdust, and Chinese Parasol Tree leaf at different ashing temperatures.

Chemical Composition Analysis

The chemical composition results of different biomass ashes determined by XRF analysis are presented in Table 3. The measurements were carried out at least three times, and the accuracy of these measurements was around 3%. The coefficient of variation of each measurement was less than 2%.

Table 3 shows that SiO_2 was predominant in most of the biomass ashes. All three biomass fuels contained large amounts of potassium, which made them slag and sinter easily during the thermo-chemical conversion process. For each particular biomass, the proportions of K_2O and Na_2O , together with Cl, decreased with increased ashing temperature, mostly due to the favorable volatility of alkali metal compounds. The release rate of Cl in the form of gaseous alkali metal chlorides increases with increasing temperature (Baxter *et al.* 1998). The element Cl facilitates alkali vaporization, resulting in the vaporization of alkali metals at 815 $^{\circ}\text{C}$. Therefore, the relatively higher ashing temperature enhanced the vaporization of some mineral species and chlorides.

Table 3. Chemical Composition of Biomass Ashes Determined by XRF (wt.%)

Sample	K ₂ O	Na ₂ O	CaO	MgO	Al ₂ O ₃	P ₂ O ₅	SiO ₂	SO ₃	Fe ₂ O ₃	TiO ₂	Cl
600 °C RSA	13.46	0.93	4.46	2.14	0.25	1.94	73.26	2.41	0.49	0.05	0.57
815 °C RSA	10.83	0.81	4.65	1.67	0.22	1.67	77.01	2.65	0.31	0.03	0.13
600 °C PSA	10.40	0.67	8.26	4.92	8.73	2.46	56.38	3.42	3.87	0.51	0.24
815 °C PSA	9.85	0.56	9.87	5.56	8.51	2.14	53.17	3.28	5.89	0.56	0.15
600 °C CCA	27.55	6.18	5.59	4.81	2.75	2.90	31.82	4.85	0.83	-	12.56
815 °C CCA	24.09	5.82	6.08	7.43	2.43	3.96	34.26	5.15	0.65	-	9.95

The high ashing temperature of the corncob and peanut shell also increased the content of CaO and MgO. The present forms of Ca and Mg were likely metal cation ions connected with oxygen functional groups, which increased the reaction possibilities with SiO₂ by alkaline-earth (Xiao *et al.* 2011). Zygarlicke *et al.* (1990) suggested that CaO could react with SiO₂ between 1100 and 1700 °C to form calcium silicate, which could be catalyzed by potassium in biomass fuels.

Furthermore, the alkali metals (such as K and Na) and their related compounds formed furnace slag in the form of gaseous phases and fly ash particles. The problem of severe ash slagging in biomass-fired boilers was probably dominated by a combination of (i) attachment of fly ash particles to the bed particle surfaces; (ii) condensation of gaseous alkali species (such as KCl, KOH, K₂SO₄) on bed particles; and (iii) chemical reaction of gaseous alkali on the surfaces of thermo-chemical conversion equipment (Öhman *et al.* 2000). Thus, 600 °C was the appropriate temperature to precisely determine the ash composition. To reduce the slagging problems caused by the vaporization of alkali metal, the purification methods should be selected on the basis of the type of biomass fuel.

Mineral Phase Analysis

Because XRD spectra are complex, a computerized search-match routine was used in the crystalline mineral identification. Figure 1 shows the XRD spectra of the biomass ashes (RSA, PSA, and CCA) obtained at different ashing temperatures, indicating the presence of crystal phases and the variations in the crystal structure according to the variation in ashing temperature.

As shown in Figs. 1(a1) and (a2), the major crystalline phases in RSA were arcanite, quartz, and sylvite. Potassium existed mainly in the forms of K₂SO₄ and KCl. In comparison with the ashes formed at different temperatures, the crystal intensity of KCl decreased with the increase in temperature, suggesting that a large proportion of KCl evaporated to the gaseous phase or was converted into other compounds. The main alkali compound evaporating in RSA was KCl. Considering previous research (Nielsen *et al.* 2000; Lin *et al.* 2003), this study found that the intense volatilization of alkali chloride (Eq. 1) occurred at 600 °C RSA when the ashing temperature increased from 600 to 815 °C. The XRD results and the chemical composition results matched well, further validating the accuracy of the XRD analysis.



As shown in Figs. 1(b1) and (b2), the main components of PSA were arcanite, plagioclases, kalicinite, and periclase. Calcite, kalicinite, and fairchildite were also present at 600 °C in PSA. When the ashing temperature increased from 600 to 815 °C, kalicinite (KHCO_3) disappeared at 815 °C in PSA (Eq. 2), and calcite (CaCO_3) and fairchildite ($\text{K}_2\text{Ca}(\text{CO}_3)_2$) were not detected. In case of the PSA at 815 °C, larnite (Ca_2SiO_4) emerged, which could be explained by Eq. 3.

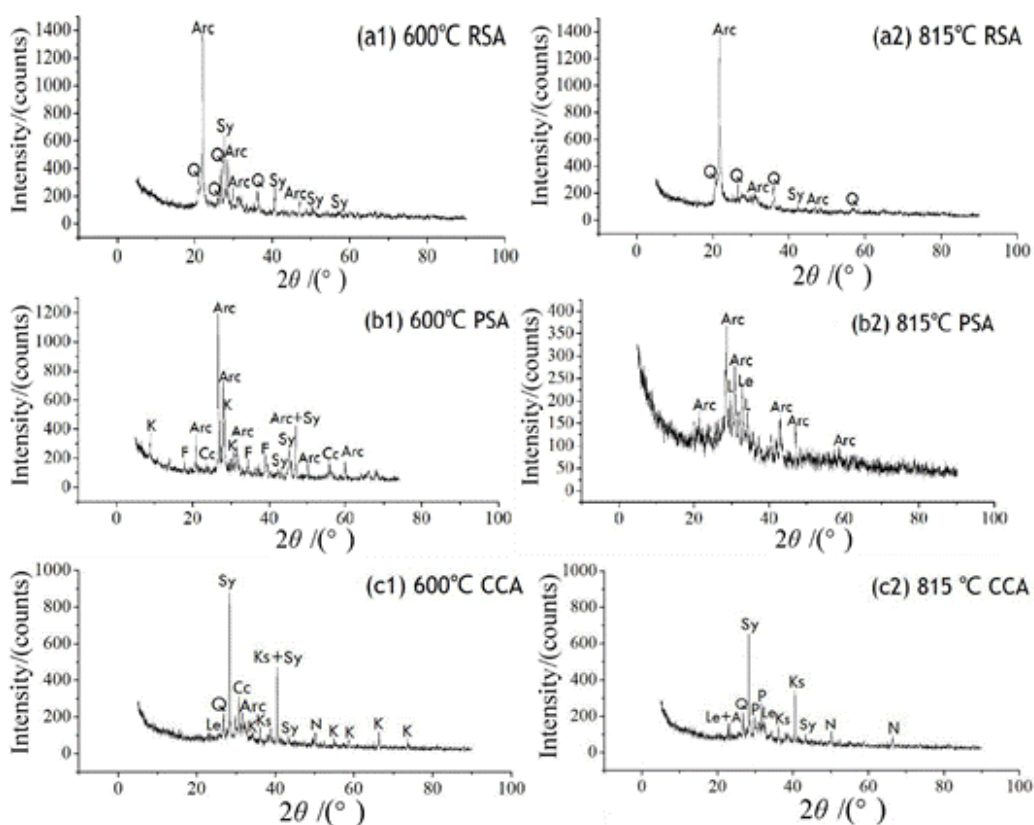


Fig. 1. X-ray diffraction patterns of (a1) 600 °C RSA, (a2) 815 °C RSA, (b1) 600 °C PSA, (b2) 815 °C PSA, (c1) 600 °C CCA, and (c2) 815 °C CCA. (Abbreviations: Arc, arcanite [K_2SO_4]; Cc, calcite [CaCO_3]; F, fairchildite [$\text{K}_2\text{Ca}(\text{CO}_3)_2$]; K, kalicinite [KHCO_3]; P, potash [K_2CO_3]; Ks, kalsilite [KAlSiO_4]; L, Larnite [Ca_2SiO_4]; Le, leucite [KAlSi_2O_6]; N, natrite [Na_2CO_3]; Q, quartz [SiO_2]; Sy, sylvite [KCl])

The XRD spectrum in Figs. 1(b1) and (b2) also shows that more complex aluminosilicates were newly formed at 815 °C, which indicated that simple minerals were gradually incorporated into complex aluminosilicates when the ashing temperature increased. The contrast of the spectra of PSA at 600 and 815 °C revealed that calcite, kalicinite, fairchildite, and sylvite—which were present in the low temperature ash—were not detected in the high temperature ash. Sylvite (KCl) disappeared in PSA at 815 °C accompanied by the presence of kalsilite (KAlSiO_4) (Eq. 4) and leucite (KAlSi_2O_6) (Eq. 5). This result was mainly due to the fact that the crystalline phases reacted with

other matter or evaporated during the ash preparation process.



As shown in Figs. 1(c1) and (c2), CCA was mainly comprised of a mixture of compounds. Potassium was present as kalcinite (KHCO_3), potash (K_2CO_3), potassium aluminum silicate (KAlSiO_4 and KAlSi_2O_6), sylvite (KCl), and arcanite (K_2SO_4). Silica was present in the form of quartz (SiO_2), and sodium was present in the form of natrite (Na_2CO_3). Figures 1(c1) and (c2) show that the XRD spectrum of CCA had one highly crystalline structure with potassium in the form of sylvite. The calcium in the CCA at 600 °C was mostly present in the form of CaCO_3 . As the temperature increased, the CaCO_3 gradually decomposed to CaO and reacted with the SiO_2 and other oxides. The reactions among CaO and SiO_2 and other oxides (Na_2CO_3 and K_2CO_3) sometimes resulted in the generation of eutectic compounds with low melting temperatures (Eqs. 6 and 7).



SEM-EDX Analysis of Biomass Ash

The surface morphology and the elemental composition of ash were analyzed by SEM-EDX after a metal spraying treatment of the ash. Figure 2 shows the images of different biomass ashes, illustrating their morphology and agglomeration characteristics. These different ash particles appeared to be irregular in shape and show agglomeration phenomena in varying degrees. The morphology and agglomeration properties of the same biomass ash at different temperatures were also different. The EDX data are listed in Table 4. For all ash samples, the predominant elements on the ash surface were C, O, Si, Cl, K, and Ca, while lesser amounts of Na, Mg, Al, P, S, and Fe were also observed.

Figure 2a(1) shows that there were some irregularly shaped floccules in the RSA at 600 °C, indicating the adhesion and slight caking of small particles. The EDX results of point a (Table 4) on the surface of the floccules showed that the carbon content was only 7.69%, while the content of Si and O were as high as 18.38% and 46.60%, respectively, revealing the fact that a large amount of SiO_2 was probably present on the surface of the floccules.

Figure 2a(2) shows the external surface of a typical agglomerate sample in RSA at 815 °C. This agglomerate sample was composed of many softening floccules, and its external surface appeared very rough. The contrast between Fig. 2a(1) and Fig. 2a(2) indicated that the RSA obtained at 815 °C agglomerated more severely and combined more compactly than the RSA obtained at 600 °C. The EDS results observed at point b were different from those observed at point a. As it can be found in Table 4, the biggest difference between the surfaces observed at two points was that at point (a) some Al and Fe was observed, while Al and Fe were not detected at point (b).

Figure 2b(1) shows the original and fibrous texture of a piece of unburnt ash particle with a large size of greater than 100 μm , indicating the inadequate combustion of peanut shells at 600 °C. The EDX results at point c demonstrated a high carbon content on the surface of the unburnt ash particles, reaching up to 39.99% (Table 4). This further verified the fact that there still existed unburnt carbon residues in 600 °C ash.

When the ashing temperature was increased, however, the unburnt particles were

not observed (Fig. 2b(2)), indicating that the peanut shells had burned out at 815 °C. Moreover, as seen in Fig. 2b(2), some quadrate crystal phases appeared. The EDX results for point d showed that Si and O were the two most abundant element species on the surface of crystal phases; hence it was inferred that most of these crystal phases were quartz. Park *et al.* (2003) suggested that SiO₂ was in the amorphous state under 800 °C, and only when temperature exceeded 900 °C could the SiO₂ with microcrystal structures be transformed into the crystal from the amorphous state.

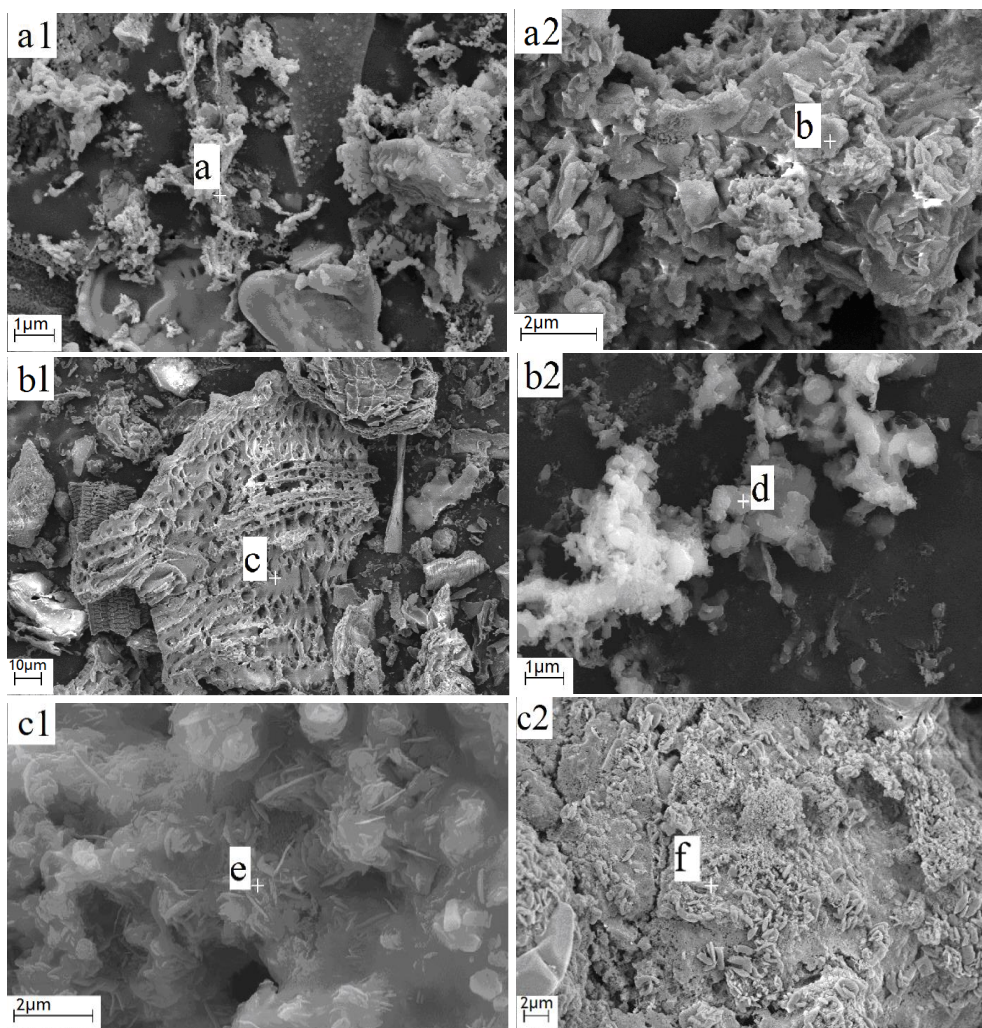


Fig. 2. SEM images of the surface morphology of (a1) rice straw ash at 600 °C, (a2) rice straw ash at 815 °C, (b1) peanut shell ash at 600 °C, (b2) peanut shell ash at 815 °C, (c1) corn cob ash at 600 °C, and (c2) corn cob ash at 815 °C. (The locations chosen for the EDX spot analyses were marked as a-f, which were shown on these provided images by a “+” for clearly identifying the exact spots of the SEM images)

Figure 2c(1) shows details of a fused zone in the CCA at 600 °C, and this zone appeared to be molten and re-solidified. A closer examination of Fig. 2c(1) showed that some partially molten or non-molten ash inclusions were still visible within the fused materials. The melting of the coating material could be the key reason for the formation of a sticky layer on the ash particles, causing the severe agglomeration and ash slagging problems. As determined by EDX (Table 4), this molten layer was particularly rich in

potassium and chlorine; thus, it was inferred that the surfaces of these molten materials were mostly coated with potassium chloride.

Figure 2c(2) shows a selected zone of the external surface of an agglomerate sample of CCA at 815 °C. Two different zones of the agglomerate were distinguished. In the first zone, the non-molten and partially molten particles appeared to be embedded in the molten layer. In the second zone, the surface seemed to be rough and compact. The EDX results of point f (Table 4) showed that the content of K decreased greatly with the increase in temperature. In addition, the content of Cl on the agglomerate surface was close to zero (0.65%), while it increased to 34.87% on the surface of the molten materials (Table 4), indicating that the alkali chlorides were most likely transferred by random collisions between ash and burning char particles.

Table 4. Results of EDX Spot Analyses in Points a through h of Fig. 2. (wt.%)

Point	C	O	Na	Mg	Al	Si	P	S	Cl	K	Ca	Fe
a	7.69	46.60	1.61	1.57	7.60	18.38	1.17	0.57	0.42	8.81	2.48	3.09
b	4.07	47.08	1.11	0.88	-	30.71	0.06	0.15	0.21	9.61	5.97	0.15
c	51.02	15.24	0.05	0.46	0.96	21.94	-	-	-	7.52	2.25	0.56
d	4.18	39.87	0.01	0.28	0.15	50.17	-	-	0.01	4.39	0.68	0.26
e	1.67	14.20	0.22	0.30	-	2.82	0.04	-	34.87	45.90	0.25	-
f	-	46.83	0.59	2.10	0.07	9.48	11.60	0.34	0.65	24.12	4.22	-

Therefore, from the above analyses, it can be found that the impacts of ashing temperature on the morphology and agglomeration properties of various biomass ashes were straightforward. As for a particular biomass, the ash agglomeration tendency was remarkably enhanced at relatively higher ashing temperatures because it was easier to reach low-melting point eutectics on the inert particle surface. The results reported in this study were qualitatively similar to those reported by Salour *et al.* (1993) and Liu *et al.* (2009) for a series of other biomass fuels. Neither biomass species, ashing temperature, nor elemental composition of ash particles had noticeable effects on the morphology and agglomeration properties.

STA Analyses of Biomass Ash Fusion Process

Figures 3 to 5, respectively shows the TG-DTG-DTA curves of RSA, PSA, and CCA being heated at the heating rate of 20 °C/min, from which the ash fusion processes of various biomass ashes obtained at different ashing temperatures can be clearly seen.

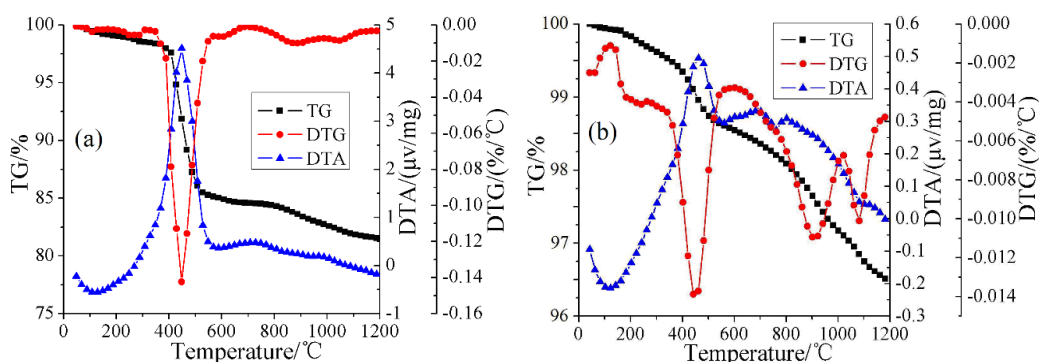


Fig. 3. Thermal analysis curves of (a) 600 °C RSA, (b) 815 °C RSA

In general, for the ash samples obtained at 600 °C, the results exhibited a total weight loss of 18.46% for the RSA at 600 °C (Fig. 3(a)), and 37.14% for the PSA at 600 °C (Fig. 4(a)) when they were heated to 1200 °C. The CCA at 600 °C had a maximum weight loss of 50.06% (Fig. 5(a)). For the same biomass fuel, the ash obtained at 600 °C exhibited greater weight loss than did the ash at 815 °C. This indicated that the total weight loss of the same biomass ash decreased with the increase of ashing temperature, corresponding well with the phase transitions and the thermal reaction sequences.

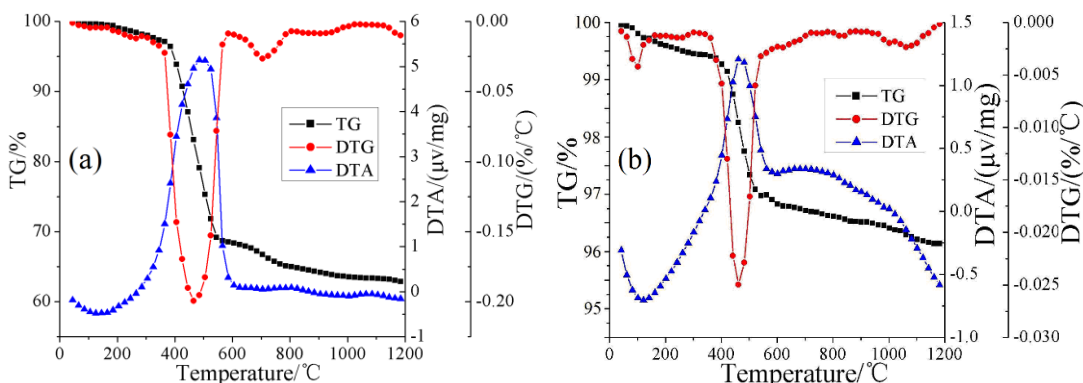


Fig. 4. Thermal analysis curves of (a) 600 °C PSA, (b) 815 °C PSA

As shown in Figs. 3 to 5, the thermal decomposition of all ashes showed stepwise mechanisms and mainly occurred in four steps. The evaporation of unbound moisture and the degradation of thermally unstable matter occurred below 200 °C. The oxidation of most organic matters occurred between 200 and 600 °C, the removal and reaction of inorganic matters occurred between 600 and 800 °C, and the thermal transformation of residual inorganic matters occurred over 800 °C.

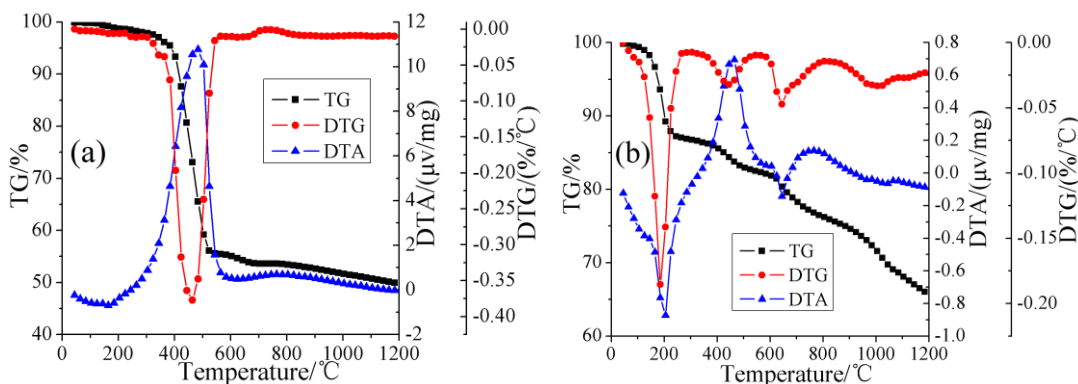


Fig. 5. Thermal analysis curves of (a) 600 °C CCA, (b) 815 °C CCA

For RSA (Figs. 3(a) and (b)), part of the weight loss occurred between 662 and 500 °C, accompanied by a sharp weight loss peak, which mainly occurred due to the volatilization of unburnt carbon and phosphorus oxides. The remaining weight loss that occurred over 700 °C was mainly attributed to KCl vaporization (Batra *et al.* 2008). As it can be seen in Fig. 3(b), there was an apparent DTG peak above 800 °C, caused mainly by the evaporation and fusion of residual inorganic substances. The thermal behavior of PSA (Figs. 4(a) and (b)) was the same as that of RSA.

Because of the exothermic reactions among these residual substances, a sharp exothermic peak appeared between 400 and 500 °C in the DTA curve. In particular, the weight losses of 815 °C RSA (Fig. 3(b)) and 815 °C CCA (Fig. 5(b)) were continuous when exceeding 1000 °C. This was mainly due to the volatilization and fusion of high-temperature molten materials in ash.

Moreover, as for 815 °C CCA (Fig. 5(b)), a small weight loss peak appeared near 650 °C in the DTG curve, accompanied by an endothermic peak in the DTA curve. As revealed by the XRD spectra, the CCA contained a large amount of KCl. As the main volatile matter in CCA, KCl could play an important role during the process of thermal pyrolysis (Abraham *et al.* 2013). This endothermic peak near 650 °C was therefore primarily caused by the melting of KCl.

Potential Utilizations of Biomass Ash

Based on the above characteristics of various biomass ashes as well as previous peer-reviewed investigations (Xiao *et al.* 2011; Abraham *et al.* 2013; Burgos *et al.* 2016), it appeared that the biomass ash was the combination of metallic oxides and silica, similar to the raw materials used for producing silicate ceramic products in the traditional ceramic industry. The ashes generated from rice straws and peanut shells could be utilized to produce high quality glasses because these two biomass ashes had appreciable silica content in addition to various oxides that were useful in glass production. Doweidar *et al.* (2009) reported that the density and hardness of the soda-lime-silica glass composition that incorporated RSA exhibited higher values than the glass ceramics using industrial chemicals. In addition, Huang *et al.* (2011) suggested that the RSA could potentially be used as a remediation treatment for soils contaminated by Cu or other heavy metals because RSA can suppress the movement and bioavailability of Cu in soils.

As determined by XRF analysis, these agricultural residue ashes had a large quantity of nutrient elements (mostly K, Ca, and P). Thus, they were suitable for use in agricultural soil to sequester carbon and enhance plant growth by supplying and retaining nutrients. Also, these biomass ashes could be used as amendments to selectively improve the physical and biological properties of agricultural soil through the selection of specific biomass and ashing conditions. When increasing the ashing temperature, the chemical composition results revealed that the contents of alkaline earth metals (Ca and Mg) increased noticeably, while the total contents of alkali metals (K and Na) and Cl decreased. Additionally, the presence of CaO made it possible for the ash to capture SO₂ (Abraham *et al.* 2013). Moreover, the volatile materials released during the ashing process created a large amount of pores in the carbonaceous materials, indicating that low-cost adsorbent could be developed from the carbon residues separated from biomass ashes. Activation produced high yields of activated carbon.

For a particular biomass fuel, the thermal analysis showed that the total weight loss of 600 °C ash was higher than that of 815 °C ash. In accordance with Abraham *et al.* (2013), the high weight loss necessitated the ash beneficiation process, whereby the magnetic material, carbon, and alkaline compounds were removed. Hence, the high silica content in the resultant ashes made possible their use as building materials in concrete and other applications. These biomass ashes, especially the ashes formed at relatively low temperatures, would be good candidates for the production of blended cement concrete.

When considering the different ashing temperatures of the different biomasses, 600 °C was the optimal temperature for biomass ash analysis in industrial applications and for precisely determining the ash properties. Moreover, these biomass ashes (RSA,

PSA, and CCA) were devoid of toxic metals, thus opening the possibility of their use as clarification in industries. Nevertheless, the applications of biomass ash for clarification have not been explored and would need further study in future research.

CONCLUSIONS

This study investigated the impacts of biomass species and ashing temperature on the physical and chemical properties of biomass ash at different temperatures. The results indicated that for a given biomass, increasing the ashing temperature caused the ash yield and the K, Na, Cl contents to decrease, but caused the Ca, Mg contents to increase. X-ray diffraction results showed the presence of crystal phases and the variation in crystal structures. Scanning electron microscopy images revealed that the ash slagging tendency was enhanced at high temperatures. The melting of the coating material on ash particles was identified as the key reason for development of a sticky layer on ash surface. Energy-dispersive X-ray data revealed that the molten materials were primarily coated with potassium chloride. Thermal analysis implied that the total weight loss of the same biomass ash decreased as ashing temperature increased, corresponding well with phase transitions and thermal reaction sequences.

ACKNOWLEDGMENTS

The authors are grateful for the support of Rural Energy Comprehensive Construction Fund of the Ministry of Agriculture of China (Grant No. 2015-36).

REFERENCES CITED

- Abraham, R., George, J., Thomas, J., and Yusuff, K. K. M. (2013). "Physicochemical characterization and possible applications of the waste biomass ash from oleoresin industries of India," *Fuel* 109, 366-372. DOI: 10.1016/j.fuel.2013.02.067
- Arvelakis, S., Jensen, P. A., and Dam-Johansen, K. (2004). "Simultaneous thermal analysis (STA) on ash from high-alkali biomass," *Energy Fuels* 18(4), 1066-1076. DOI: 10.1021/ef034065
- ASTM E1755-01 (2015). "Standard test method for ash in biomass," ASTM International, West Conshohocken, PA, USA.
- Baxter, L. L., Miles, T. R., Miles, T. R., Jr., Jenkins, B. M., Milne, T., Dayton, D., Bryers, R. W., and Oden, L. L. (1998). "The behavior of inorganic material in biomass-fired power boilers: Field and laboratory experiences," *Fuel Processing Technology* 54(1-3), 47-78. DOI: 10.1016/S0378-3820(97)00060-X
- Batra, V. S., Urbonaite, S., and Svensson, G. (2008). "Characterization of unburned carbon in bagasse fly ash," *Fuel* 87(13-14), 2972-2976. DOI: 10.1016/j.fuel.2008.04.010
- Blissett, R. S., and Rowson, N. A. (2012). "A review of the multi-component utilisation of coal fly ash," *Fuel* 97, 1-23. DOI: 10.1016/j.fuel.2012.03.024
- Burgos, N., Valdes, A., and Jimenez, A. (2016). "Valorization of agricultural wastes for the production of protein-based biopolymers," *Journal of Renewable Materials* 4(3),

- 165-177. DOI: 10.7569/JRM.2016.634108
- Doweidar, H., El-Damrawi, G., El-Egili, K., Moustafa, Y., Ramadan, R. M., Abdelghany, M., and Kamal, H. (2009). "Rice straw ash as a raw material for glass production," *Glass Technology – European Journal of Glass Science and Technology Part A* 50(4), 196-202.
- Fang, X., and Jia, L. (2012). "Experimental study on ash fusion characteristics of biomass," *Bioresource Technology* 104, 769-774. DOI: 10.1016/j.biortech.2011.11.055
- GB/T212-2008 (2008). "Proximate analysis of coal," Chinese National Bureau of Standards, Beijing, China.
- Haykiri-Acma, H., Yaman, S., and Kucukbayrak, S. (2013). "Production of biobriquettes from carbonized brown seaweed," *Fuel Processing Technology* 106(2), 33-40. DOI: 10.1016/j.fuproc.2012.06.014
- Huang, J. H., Hsu, S. H., and Wang, S. L. (2011). "Effects of rice straw ash amendment on Cu solubility and distribution in flooded rice paddy soils," *Journal of Hazardous Materials* 186(2-3), 1801-1807. DOI: 10.1016/j.jhazmat.2010.12.066
- Knudsen, J. N., Jensen, P. A., and Dam-Johansen, K. (2004). "Transformation and release to the gas phase of Cl, K, and S during combustion of annual biomass," *Energy and Fuels* 18(5), 1385-1399. DOI: 10.1021/ef049944q
- Kutchko, B. G., and Kim, A. G. (2006). "Fly ash characterization by SEM-EDS," *Fuel* 85(17-18), 2537-2544. DOI: 10.1016/j.fuel.2006.05.016
- Liao, S. W., Lin, C. I., and Wang, L. H. (2011). "Kinetic study on lead (II) ion removal by adsorption onto peanut hull ash," *Journal of the Taiwan Institute of Chemical Engineers* 42(1), 166-172. DOI: 10.1016/j.jtice.2010.04.009
- Lin, W. G., Dam-Johansen, K., and Frandsen, F. (2003). "Agglomeration in bio-fuel fired fluidized bed combustors," *Chemical Engineering Journal* 96(1-3), 171-185. DOI: 10.1016/j.cej.2003.08.008
- Liu, Y. S., Zheng, L. T., Li, X. D., and Xie, S. D. (2009). "SEM/EDS and XRD characterization of raw and washed MSWI fly ash sintered at different temperatures," *Journal of Hazardous Materials* 162(1), 161-173. DOI: 10.1016/j.jhazmat.2008.05.029
- McKendry, P. (2002). "Energy production from biomass (Part 2): Conversion technologies," *Bioresource Technology* 83(1), 47-54. DOI: 10.1016/S0960-8524(01)00119-5
- Motghare, K. A., Rathod, A. P., Wasewar, K. L., and Labhsetwar, N. K. (2016). "Comparative study of different waste biomass for energy application," *Waste Management* 47(A), 40-45. DOI: 10.1016/j.wasman.2015.07.032
- Nielsen, H. P., Baxter, L. L., Sclippab, G., Morey, C., Frandsen, F. J., and Dam-Johansen, K. (2000). "Deposition of potassium salts on heat transfer surfaces in straw-fired boilers: a pilot-scale study," *Fuel* 79(2), 131-139. DOI: 10.1016/S0016-2361(99)00090-3
- Öhman, M., Nordin, A., Skrifvars, B. J., Backman, R., and Hupa, M. (2000). "Bed agglomeration characteristics during fluidized bed combustion of biomass fuels," *Energy and Fuels* 14(1), 169-178. DOI: 10.1021/ef990107b
- Ogundiran, M. B., Babayemi, J. O., and Nzeribe, C. G. (2011). "Determination of metal content and an assessment of the potential use of waste cashew nut ash (CNSA) as a source for potash production," *BioResources* 6(1), 529-536. DOI: 10.15376/biores.6.1.529-536
- Pan, H., and Eberhardt, T. L. (2011). "Characterization of fly ash from the gasification of

- wood and assessment for its application as a soil amendment,” *BioResources* 6(4), 3987-4004. DOI: 10.15376/biores.6.4.3987-4004
- Park, B. D., Wi, S. G., Lee, K. H., Singh, A. P., Yoon, T. H., and Kim, Y. S. (2003). “Characterization of anatomical features and silica distribution in rice husk using microscopic and micro-analytical techniques,” *Biomass Bioenergy* 25(3), 319-327. DOI: 10.1016/S0961-9534(03)00014-X
- Quaranta, N., Unsen, M., Lopez, H., Giansiracusa, C., Roether, J. A., and Boccaccini, A. R. (2011). “Ash from sunflower husk as raw material for ceramic products,” *Ceramics International* 37(1), 377-385. DOI: 10.1016/j.ceramint.2010.09.015
- Rehrah, D., Reddy, M. R., Novak, J. M., Bansode, R. R., Schimmel, K. A., Yu, J., Watts, D. W., and Ahmedna, M. (2014). “Production and characterization of biochars from agricultural by-products for use in soil quality enhancement,” *Journal of Analytical and Applied Pyrolysis* 108, 301-309. DOI: 10.1016/j.jaap.2014.03.008
- Rizvi, T., Xing, P., Pourkashanian, M., Darvell, L. I., Jones, J. M., and Nimmo, W. (2015). “Prediction of biomass ash fusion behaviour by the use of detailed characterisation methods coupled with thermodynamic analysis,” *Fuel* 141, 275-284. DOI: 10.1016/j.fuel.2014.10.021
- Salour, D., Jenkins, B. M., Vafaei, M., and Kayhanian, M. (1993). “Control of in-bed agglomeration by fuel blending in a pilot scale straw and wood fueled AFBC,” *Biomass and Bioenergy* 4(2), 117-133. DOI: 10.1016/0961-9534(93)90033-Z
- Skrifvars, B. J., Lauren, T., Hupa, M., Korbee, R., and Ljung, P. (2004). “Ash behaviour in a pulverized wood fired boiler – A case study,” *Fuel* 83(10), 1371-1379. DOI: 10.1016/j.fuel.2004.01.008
- Terzioğlu, P., Yucel, S., Rabagah, T. M., and Özçimen, D. (2013). “Characterization of wheat hull and wheat hull ash as a potential source of SiO₂,” *BioResources* 8(3), 4406-4420. DOI: 10.15376/biores.8.3.4406-4420
- Wang, S., Jiang, X. M., Han, X. X., and Wang, H. (2008). “Fusion characteristic study on seaweed biomass ash,” *Energy Fuels* 22(4), 2229-2235. DOI: 10.1021/ef800128k
- Xiao, R. R., Chen, X. L., Wang, F. C., and Yu, G. S. (2011). “The physicochemical properties of different biomass ashes at different ashing temperatures,” *Renewable Energy* 36(1), 244-249. DOI: 10.1016/j.renene.2010.06.027
- Zygarlicke, C. J., Steadman, E. N., and Benson, S. A. (1990). “Studies of transformations of inorganic constituents in a Texas lignite during combustion,” *Progress in Energy and Combustion Science* 16, 195-204. DOI: 10.1016/0360-1285(90)90028-2

Article submitted: November 25, 2016; Peer review completed: March 3, 2017; Revised version received and accepted: March 7, 2017; Published: March 15, 2017.

DOI: 10.15376/biores.12.2.3222-3235